Data Analysis of Diagonally Connected Magnetohydrodynamic Power Generator Experiments

Carlson C. P. Pian*
Avco Research Laboratory, Inc., Everett, Massachusetts

The data from diagonally connected MHD generator experiments at the Avco Mk VI facility and at the Component Development and Integration Facility have been compared with computer analyses. The results of the comparisons were used to study the slagging effects on the generator performance as a function of the various operating conditions. The cathode interelectrode voltage nonuniformity was found to be the most important effect in reducing the effective axial slag impedance of the generator. An electrical model of the diagonally connected MHD generator with external linkage resistors was formulated to assist in the data analysis. The electrical model has been described.

Nomenclature

B = magnetic field intensity, T
D = channel width, m
E = electric field, V/m
H = channel height, m
I = electric current, A
J = electric current density, A/m^2
L = channel length, m
$\dot{m}$ = mass flow rate, kg/s
N = number of overlapped electrodes
p = length of electrode-insulator pitch, m
P_{MHD} = MHD power output, MWe
R = electrical resistance, Ω
S = slag layer thickness, m
u = gas velocity, m/s
V_{arc} = arc voltage drop, V
V_{Hall} = Hall voltage, V
β = Hall parameter
δ = boundary layer thickness, m
Θ = electrode overlap angle, deg
σ = gas conductivity, mho/m

Subscripts

c = core flow value
cr = corner flow region
ew = electrode wall
LD = load
LK = link
s = slag
sew = electrode wall slag layer
ssw = sidewall slag layer
sw = sidewall
x = axial direction
y = transverse direction

Introduction

THE data from diagonally connected MHD generator experiments at the Avco Mk VI facility[1,2] and at the U.S. Department of Energy's Component Development and Integration Facility (CDIF)[3,4] have been compared with analyses. The present investigation focuses on the effects of slag on generator performance as a function of the operating conditions. The slag coatings on the generator walls can decrease the surface heat and voltage drop losses. However, the slag layers, which are electrically conducting, can also lower the end-to-end resistance of the generator, thus degrading the generator's performance. Cathode nonuniformities can also affect the performance of the MHD generator. These nonuniformities in the interelectrode voltage distribution originate at the cathode wall when groups of electrodes are shorted by polarized slag coatings.[5,6] The cause of the elevated cathode slag layer conductivity is thought to be from the congregation of potassium or iron and iron oxide compounds within sections of the slag layer, driven there by the generated electric field.[7] The shorted cathode slag layer is periodically "broken" by Joule heating due to current concentrations.[8] The resulting change in the effective segmentation of the cathode wall causes a few insulator gaps to sustain the total Hall voltage of the generator. Normally, in the absence of cathode nonuniformities, this accumulated Hall voltage would divide approximately equally over all the cathode interelectrode gaps.

In the present study, the following questions were investigated: how much is the diagonal generator performance influenced by slag, and what factors affect the effective slag layer resistance under actual power generation conditions? The experimental data from past diagonal generator testings for different values of the oxidant nitrogen/oxygen ratio (N/O), magnetic field intensity, and external loading were compared to the results of computer simulations. From these comparisons, the slag layer resistivity can be inferred as a function of the various generator operating parameters.

A special feature of the Avco and CDIF diagonal generator experiments has been the placement of resistors in the external diagonal links to serve as crude current controllers. Current controllers are needed for slagging diagonal generators in order to protect the anode walls from the cathode voltage nonuniformities. Without these resistors, the high cathode voltage spikes would reflect along the shorted diagonal links onto the anode wall and lead to interanode arcing. When interelectrode arcs appear on the cathode wall, the Lorentz body forces would push the arcs out into the plasma core flow region where they will be extinguished without causing any damage to the channel wall. However, when the arcs appear on the anode wall, these same body forces would force the arcs into the interelectrode insulators. If no control is used, however crude, severe and potentially damaging anode faults would result. The linkage resistors are not suitable for powerplant applications because they can

Received Jan. 9, 1986; revision received June 16, 1986.

*Principal Research Engineer, Energy Technology Office. Member AIAA.

dissipate an appreciable amount of the generated power. Nondissipative electrode current control circuits will eventually take over the blocking function of these resistors. However, the unavailability of current control devices to outfit a complete channel necessitates the use of linkage resistors in near-term test programs.

To aid in the data analysis, an electrical model of the diagonally connected MHD generator with link resistors has been formulated. This electrical model is described in the first part of this paper. The electrical model has been incorporated into a performance prediction code and was used to analyze the data from diagonally loaded generator experiments. The comparisons of analyses with measurements are presented in the second half of this paper.

For the purpose of quantifying the impact of slag on generator performance, the following parameter for effective slag layer resistance is defined

$$(\mathrm{Eff}R)_{\mathrm{slag}} = \frac{p}{2S\langle\sigma\rangle_s (D+H)} \tag{1}$$

where p is the electrode pitch, S the slag layer thickness, $\langle\sigma\rangle_s$ the value of slag layer electrical conductivity used in the analysis, and D and H the midchannel values of the generator width and height, respectively. $(\mathrm{Eff}R)_{\mathrm{slag}}$ has units of ohms per interelectrode gap. In the analysis, *all* the different slag layer effects on the generator performance are lumped into the equivalent (4-wall) slag layer resistance of Eq. (1). The slagging effects, which influence the value of $(\mathrm{Eff}R)_{\mathrm{slag}}$, as well as their relative importance are subsequently identified in the comparison between calculated and measured results. The present formulation of slag layer effects differs from that reported in Refs. 9 and 10, where slag behaviors on cathode, anode, and sidewalls are modeled separately. The latter modeling approach, being more complicated and having more adjustable constants and parameters, was found to be less suitable for the present investigation.

Electrical Model of Diagonally Connected MHD Generator with Link Resistors

An electrical model of the diagonally connected MHD generator with external link resistors is described in this section. The model seeks the approximate electric solution of the MHD generator instead of exactly solving the Maxwell's equations and the Ohm's law throughout the calculational domain. The latter approach is more lengthy and can substantially increase the computational cost. The electrical model must be combined with a fluid-dynamic model of the MHD generator. The fluid model is not discussed here. The present electrical model was developed to be used in conjunction with a coupled core/boundary layer MHD flow model.[11]

The MHD generator cross section is divided into core, boundary layer, slag layer, and corner regions, as shown in Fig. 1. The electrical solutions of the MHD generator are obtained from a closed set of equations, which resulted from the description of the electrical connections and from the averaging of the electrical distributions in the various regions shown in Fig. 1. The distributions of the electrical variables in these regions are determined such that Ohm's law is satisfied along with the following approximations.

Core Flow Region

The electrical and gasdynamic variables in the core region are assumed constant at each streamwise x location; thus, from Ohm's law,

$$J_{xc} = \sigma_c E_{xc} - \beta_c J_{yc} \tag{2}$$

$$E_{yc} = -\beta_c E_{xc} + \left(\frac{1+\beta_c^2}{\sigma_c}\right) J_{yc} + u_c B \tag{3}$$

Electrode Wall Boundary Layer Regions

The electrode walls are assumed to be infinitely segmented. Under such conditions, the transverse variations of the Hall field and Faraday current density are small. Consequently, E_x and J_y in the electrode wall boundary layer regions are set equal to their respective core values

$$E_{xew} = E_{xc} \tag{4}$$

$$J_{yew} = J_{yc} \tag{5}$$

The remaining electrical variables (E_{yew} and J_{xew}) can be determined from Ohm's law. They are averaged across the electrode wall boundary layer thickness δ_{ew} to get

$$\langle E_y\rangle_{ew} = -\langle\beta\rangle_{ew} E_{xc} + \left\langle\frac{1+\beta^2}{\sigma}\right\rangle_{ew} J_{yc} + \langle u\rangle_{ew} B \tag{6}$$

$$\langle J_x\rangle_{ew} = \langle\sigma\rangle_{ew} E_{xc} - \langle\beta\rangle_{ew} J_{yc} \tag{7}$$

where

$$\langle f\rangle_{ew} = \frac{1}{\delta_{ew}} \int_0^{\delta_{ew}} f(y)\,\mathrm{d}y \tag{8}$$

The effects of current transport by concentrated arcs are included in the terms involving σ in Eqs. (6) and (7). Arcing is assumed to occur when the local value of E_y in the electrode wall boundary layer becomes greater than some specified amount (typically chosen to be -10 kV/m). The electrical conductivity of the gas is then frozen from that point on as one proceeds through the boundary layer towards the wall.

Sidewall Boundary Layer Regions

The sidewalls of the MHD generator are assumed to be electrically insulating, so that the core electric field is imposed onto the sidewall boundary layer regions

$$E_{xsw} = E_{xc} \tag{9}$$

$$E_{ysw} = E_{yc} \tag{10}$$

The current densities, determined from Ohm's law and averaged over δ_{sw}, are

$$\langle J_x\rangle_{sw} = \left(\left\langle\frac{\sigma}{1+\beta^2}\right\rangle_{sw} + \beta_c\left\langle\frac{\sigma\beta}{1+\beta^2}\right\rangle_{sw}\right)E_{xc} - \frac{1+\beta_c^2}{\sigma_c}\left\langle\frac{\sigma\beta}{1+\beta^2}\right\rangle_{sw} J_{yc} + \left(\left\langle\frac{u\sigma\beta}{1+\beta^2}\right\rangle_{sw} - u_c\left\langle\frac{\sigma\beta}{1+\beta^2}\right\rangle_{sw}\right)B \tag{11}$$

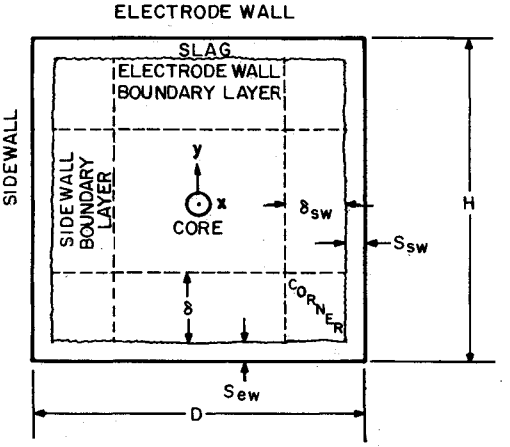

Fig. 1 Channel cross section for electrical model.

$$\langle J_y\rangle_{sw}=\left(\left\langle\frac{\sigma\beta}{1+\beta^2}\right\rangle_{sw}-\beta_c\left\langle\frac{\sigma}{1+\beta^2}\right\rangle_{sw}\right)E_{xc}$$
$$+\frac{1+\beta_c^2}{\sigma_c}\left\langle\frac{\sigma}{1+\beta^2}\right\rangle_{sw}J_{yc}$$
$$+\left(u_c\left\langle\frac{\sigma}{1+\beta^2}\right\rangle_{sw}-\left\langle\frac{\sigma u}{1+\beta^2}\right\rangle_{sw}\right)B \qquad (12)$$

where $\langle\ \rangle_{sw}$ is defined as

$$\langle f\rangle_{sw}=\frac{1}{\delta_{sw}}\int_0^{\delta_{sw}}f(z)\mathrm{d}z \qquad (13)$$

The possibility of velocity overshoots in the sidewall boundary layers are taken into account in this model through the transverse variation of $u(z)$.

Corner Flow Regions

For the corner regions, the following assumptions are made:

$$\langle J_y\rangle_{cr}=\langle J_y\rangle_{sw} \qquad (14)$$

$$E_{xcr}=E_{xc} \qquad (15)$$

Equation (14) preserves current conservation; Eq. (15) ensures that the electric fields in the corners are consistent with those in the electrode wall and sidewall boundary layer regions. The remaining electrical variables are determined from Ohm's law. The averaged axial current density in the corner regions is

$$\langle J_x\rangle_{cr}=\langle\sigma\rangle_{cr}E_{xc}-\langle\beta J_y\rangle_{cr} \qquad (16)$$

where the corner averages are approximated by

$$\langle\beta J_y\rangle_{cr}\approx\langle\beta\rangle_{cr}\langle J_y\rangle_{cr}$$
$$\langle\beta\rangle_{cr}\approx\langle\beta\rangle_{ew}\langle\beta\rangle_{sw}/\beta_c$$
$$\langle\sigma\rangle_{cr}\approx\langle\sigma\rangle_{ew}\langle\sigma\rangle_{sw}/\sigma_c$$

Electrode Wall Slag Layer Regions

The slag layer is modeled as a viscous wall layer driven by the shear force of the gas flow and balanced against the viscosity distribution within the layer. The viscosity distribution across the layer is defined by the local heat transfer and assumed slag properties. The distributions of the electrical variables in the slag layers are determined from electrical conditions imposed by the boundary layer regions immediately above the slag layers. For the slag layers on the electrode walls, values of axial electric field and transverse current density are imposed from the regions above

$$E_{xsew}=E_{xew}=E_{xc} \qquad (17)$$

$$J_{ysew}=J_{yew}=J_{yc} \qquad (18)$$

Averaging Ohm's law across the slag layer thickness

$$\langle J_x\rangle_{sew}=\langle\sigma\rangle_s E_{xc} \qquad (19)$$

$$\langle E_y\rangle_{sew}=\langle 1/\sigma\rangle_{sew}J_{yc} \qquad (20)$$

$\langle\sigma\rangle_s$ is the averaged slag conductivity in Eq. (1). Current transport across the slag layer by means of concentrated arcs can be modeled by assuming the transverse slag conductivity $\langle 1/\sigma\rangle_{sew}$ equals zero, i.e., no transverse diffuse current.

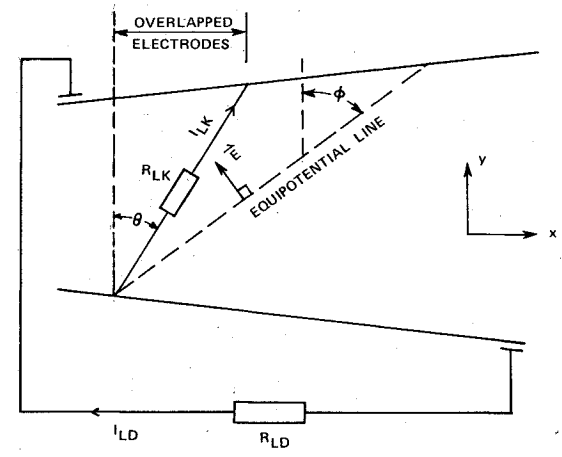

Fig. 2 Diagonally connected generator with link resistors.

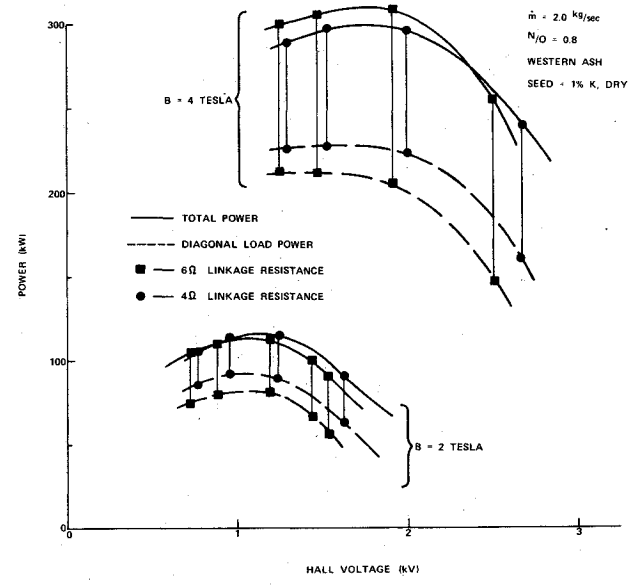

Fig. 3 Measured values of power and Hall voltage from the diagonally connected Ref. Channel No. 3 generator, N/O = 0.8.

Sidewall Slag Layer Regions

The core electric field is imposed on the sidewall slag layers, as on the sidewall boundary layers,

$$E_{xssw}=E_{xc} \qquad (21)$$

$$E_{yssw}=E_{yc} \qquad (22)$$

Averaging Ohm's law across the slag layer results in

$$\langle J_x\rangle_{ssw}=\langle\sigma\rangle_s E_{xc} \qquad (23)$$

$$\langle J_y\rangle_{ssw}=\langle\sigma\rangle_s E_{yc} \qquad (24)$$

The electric fields and current densities within the various boundary layer, corner, and slag layer regions have been expressed in terms of the core fields and core current densities [Eqs. (4-24)]. In order to solve these equations, the external loading condition and the diagonal link connections must now be imposed. These two conditions are 1) the voltage drop across the external link resistor must equal the internal voltage drop plus the arc voltage drop ($\int_\ell E\mathrm{d}\ell=0$), and 2) the sum of the currents crossing the plane formed by the overlapping electrodes (see Fig. 2) must equal the load cur-

rent ($\int_A J \mathrm{d}A = I_{LD}$). The voltage relation can be expressed as

$$I_{LK}R_{LK} = E_{yc}(H - 2\delta_{ew} - S_{ew}) + 2\langle E_y\rangle_{ew}\delta_{ew} + 2\langle E_y\rangle_{sew}S_{ew} + NPE_{xc} + V_{\text{arc}} \quad (25)$$

The link current I_{LK} is defined as the current per electrode

$$I_{LK} = -P[J_{yc}(D - 2\delta_{sw} - 2S_{sw}) + 2\langle J_y\rangle_{sw}\delta_{sw} + 2\langle J_y\rangle_{ssw}S_{sw}] \quad (26)$$

In the above equations, N is the number of overlapped electrodes, S the slag layer thicknesses, P the length of electrode-insulator pitch, H the generator height, D the generator width, and V_{arc} the arc voltage drop. The value of V_{arc} is assumed to vary linearly with the Faraday current density up to some cutoff value (typically 70 V for slagged walls) after which V_{arc} remains constant.

The load current relation can be expressed as

$$I_{LD} = H \times D \times (-\langle J_y\rangle_A \tan\Theta + \langle J_x\rangle_A) \quad (27)$$

Θ is the overlap angle as defined in Fig. 2. $\langle J_y\rangle_A$ and $\langle J_x\rangle_A$ are current densities across the generator cross section,

$$\langle J_y\rangle_A = \frac{1}{D} \times \left\{ \begin{array}{l} J_{yc}(D - 2\delta_{sw} - 2S_{sw}) \\ +2\langle J_y\rangle_{sw}\delta_{sw} \\ +2\langle J_y\rangle_{ssw}S_{sw} \end{array} \right\} \quad (28)$$

$$\langle J_x\rangle_A = \frac{1}{HD} \times \left\{ \begin{array}{l} J_{xc}(D - 2\delta_{sw} - 2S_{sw})(H - 2\delta_{ew} - 2S_{ew}) \\ +2\langle J_x\rangle_{ew}(D - 2\delta_{sw} - 2S_{sw})\delta_{ew} \\ +2\langle J_x\rangle_{sw}(H - 2\delta_{ew} - 2S_{ew})\delta_{sw} \\ +4\langle J_x\rangle_{cr}\delta_{ew}\delta_{sw} \\ +2\langle J_x\rangle_{sew}(D - 2\delta_{sw} - 2S_{sw})S_{ew} \\ +2\langle J_x\rangle_{ssw}(H - 2\delta_{ew} - 2S_{ew})S_{sw} \\ +4\langle J_x\rangle_{ssw}(\delta_{ew} + S_{ew})S_{sw} \\ +4\langle J_x\rangle_{sew}\delta_{sw}S_{ew} \end{array} \right\} \quad (29)$$

The following are all specified for the diagonally connected link resistor generator: the axial distribution of the link resistors, the number of overlapped electrodes, and the value of the load current. Equations (25-27), along with Ohm's law for the core flow region, form a closure for the core electrical solution. The electrical variables in all the other regions can then be determined once the core field and current density are known.

Data Analysis of the Avco Mk VI Reference Channel No. 3 Diagonal Generator Tests

The electrical model previously described was incorporated into an MHD generator performance analysis code[11] and was used to analyze results from two recent diagonal generator experiments. The comparison of analyses with the Avco Mk VI measurements is presented in this section. Results of the comparison with CDIF data are presented in the following section.

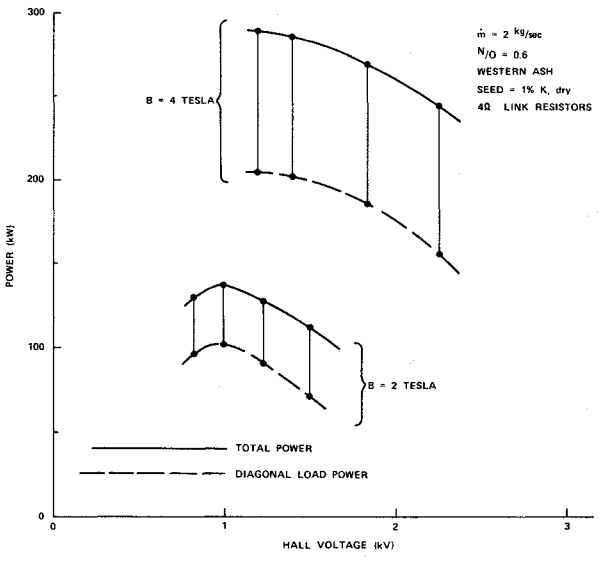

Fig. 4 Measured values of power and Hall voltage from the diagonally connected Ref. Channel No. 3 generator, N/O = 0.6.

The diagonal/link resistor experiments at Avco were performed with the Reference Channel No. 3. This channel was 2.5 m long, consisting of 140 segmented electrode pairs. The generator flow conditions in these tests varied from preliminary high subsonic flows at 4 T to shocked flows at lower values of magnetic field strength. The plasma source was a 20-MW_{th} combustor operating with oxygen-enriched air and No. 2 fuel oil. Montana Rosebud coal ash was injected for the slagging tests. The measured values of MHD power and Hall voltage are shown in Figs. 3 and 4 for two different values of N/O. The dashed lines represent the power delivered to the main diagonal load and the solid lines represent the total power dissipated outside the MHD generator by the linkage resistors and the main diagonal load. Two series of measurements were taken at the N/O = 0.8 condition for differing values of linkage resistance. Additional experimental results, as well as the details of the test conditions, can be found in Ref. 2.

The analysis of the MHD generator is based on an iterative shooting solution technique.[12] The channel geometry, magnetic field intensity, and link resistor profiles are prescribed in the analyses. The generator mass flux, N/O ratio, and the combustor/nozzle heat loss are also selected to agree with experimental values. For the analyses of situations where the Reference Channel No. 3 generator operated in the shocked flow mode, i.e., the lower B-field cases, the actual shock system is approximated by a normal shock.

Generator calculations were carried out for each of the experimental conditions. The assumed values of $(\mathrm{Eff}R)_{\text{slag}}$ and wall temperature (slag-surface temperature) were varied until the calculated MHD power output, the power delivered to the main diagonal load, the Hall voltage, and the channel heat loss all agreed with the measured values. The value of $(\mathrm{Eff}R)_{\text{slag}}$ determined in this manner may be interpreted as the effective wall leakage resistance, which has the same effect on the overall generator performance as the actual effects of slag layer leakage and cathode wall nonuniformities.

The comparison of the experimental and analytical results have helped to illustrate the importance of slagging effects on generator performance. Figures 5 and 6 compare the measured and calculated values of MHD power output and Hall voltage at $B_{\max} = 4$ T and N/O = 0.8. Results for linkage resistance of 4 ohms are shown in Fig. 5; those for resistance of 6 ohms are shown in Fig. 6. Calculated results for several assumed values of equivalent slag layer resistance and diago-

nal load current are shown. At the higher Hall voltages (or lower values of diagonal load currents), test data agree best with those calculations using higher effective slag layer resistances. Lower values of $(\mathrm{Eff}R)_{\mathrm{slag}}$ are needed for agreement at the lower Hall voltages. This trend can best be explained by the effects of cathode wall nonuniformities. The typical variations in the intercathode voltage nonuniformity patterns can be seen in Fig. 7 for several different diagonal loadings. The number of working (nonshorted) gaps that sustain the total axial voltage decreases with decreasing values of V_{Hall}. At higher values of diagonal load currents, the performance of the MHD generator is reduced as a result of the decreased number of working gaps on the cathode wall. This effect is modeled in the present calculations by using lower values of $(\mathrm{Eff}R)_{\mathrm{slag}}$ as the value of diagonal load current increases.

A rough estimate of the amount of diagonal generator performance degradation caused by slagging effects can be obtained from the calculated results such as those in Fig. 5. For example, consider the 150- and 175-A load current cases. The actual measured power outputs were about 230 kW. However, if the generator was able to operate at these same load conditions with a minimum of cathode wall slag shortings, for example, $(\mathrm{Eff}R)_{\mathrm{slag}} \simeq 3\Omega$, then the power outputs would increase to about 280 kW. The ~20% reduction in the calculated power output as $(\mathrm{Eff}R)_{\mathrm{slag}}$ is decreased from ~3 to ~0.7 Ω can be attributed to the slagging effects. The amount of Hall voltage reduction caused by slag effects can be estimated in a similar manner from Fig. 5.

Figures 8 and 9 show typical calculation/measurement comparisons in the streamwise variations of electrode current and interanode voltage. The small discrepancies between the results near the generator exit are caused by simplifications in the calculations, which resulted in some improper accounting of the grading resistors that were used in the load current consolidation circuits.

Figure 10 compares the computed with the measured values of MHD power output and Hall voltage at $B_{\max} = 4$ T and N/O = 0.6. The calculated results for several values of assumed slag layer resistances are again shown. As the Hall voltage increases, relatively lower effective slag-layer resistances are required for agreement with the measured data.

Comparing the results of Fig. 10 to the corresponding diagonal load cases in Fig. 5, a reduction in the effective slag layer resistivity is noticeable as N/O is decreased. Part of this decrease in the value of $(\mathrm{Eff}R)_{\mathrm{slag}}$ can be attributed to cathode wall nonuniformities. The measurements from experimental runs at the same diagonal load resistance indicate that the number of working gaps on the cathode wall tends to decrease with decreasing values of N/O.

Typical comparisons between the calculated and measured results at a magnetic field intensity of 2 T are shown in Fig. 11. Two Tesla results for other values of linkage resistances and N/O ratios can be found in Ref. 13. The values of

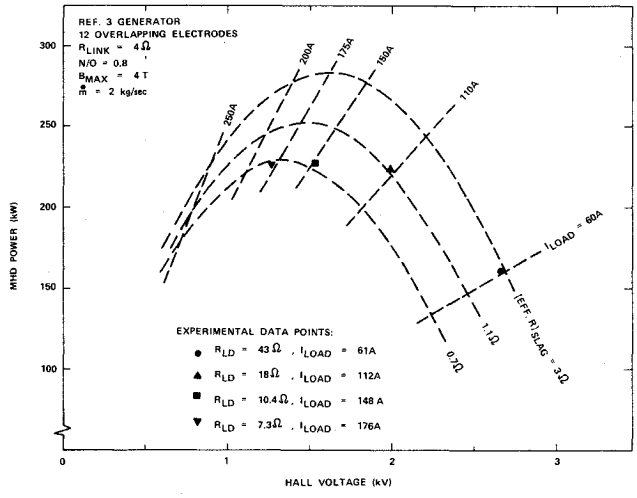

Fig. 5 MHD power vs Hall voltage; N/O = 0.8, linkage resistance = 4Ω.

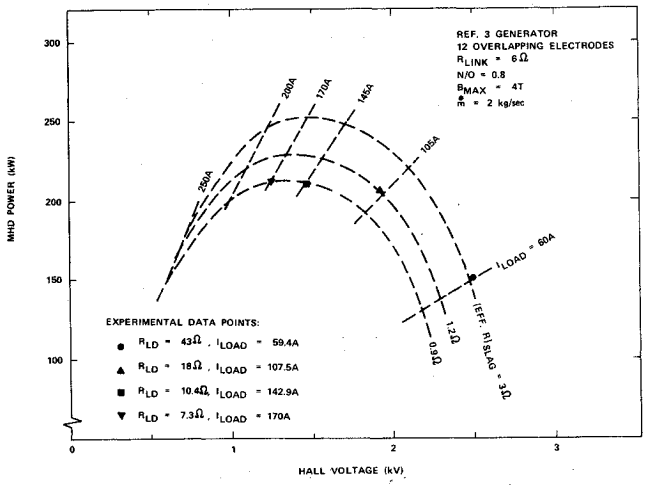

Fig. 6 MHD power vs Hall voltage; N/O = 0.8, linkage resistance = 6Ω.

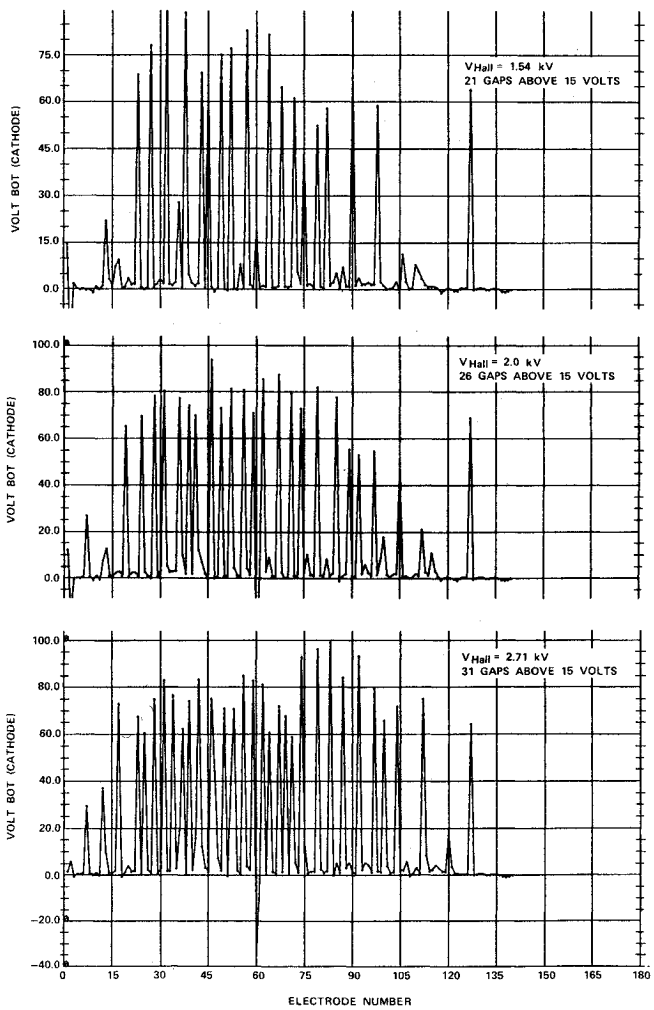

Fig. 7 Streamwise distributions of interanode voltages for different generated Hall voltages: $B_{\max} = 4$ T, N/O = 0.8, $\dot{m} = 2$ kg/s, 4 Ω linkage resistors.

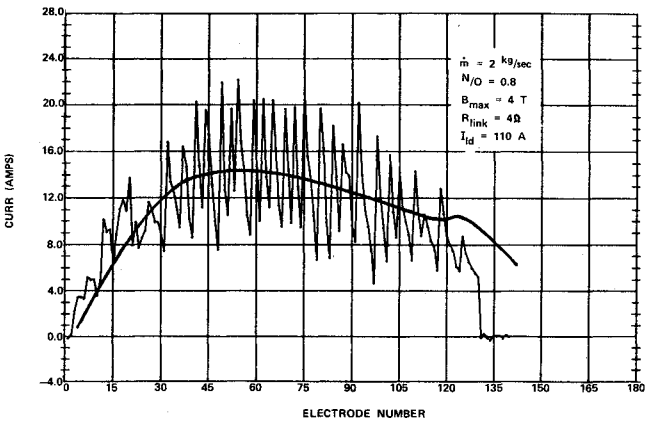

Fig. 8 Comparison of measured and calculated linkage current distributions.

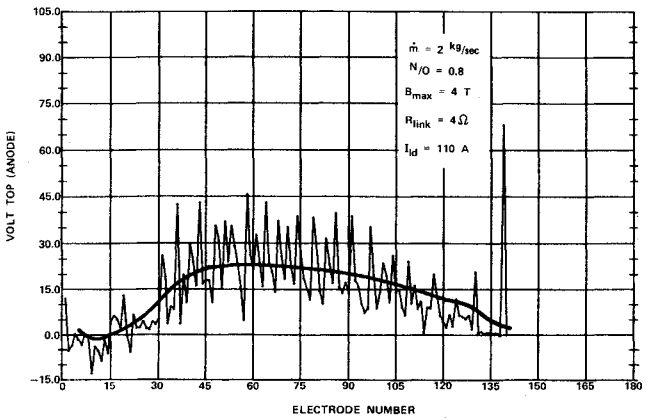

Fig. 9 Comparison of measured and calculated interanode voltage distributions.

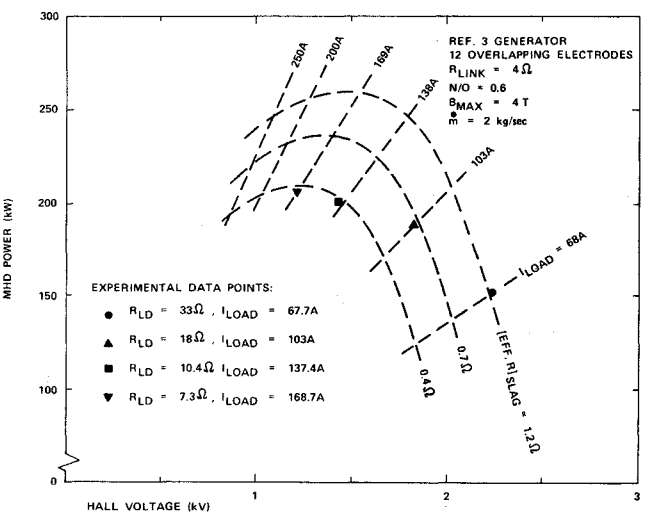

Fig. 10 MHD power vs Hall voltage; N/O = 0.6, linkage resistance = 4 Ω.

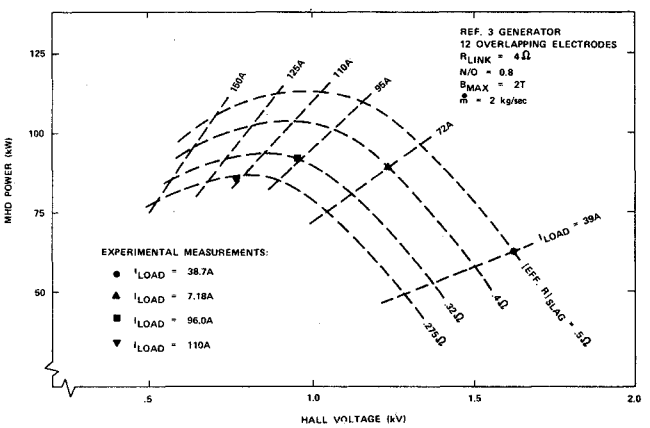

Fig. 11 MHD power vs Hall voltage; N/O = 0.8, B_{max} = 2 T.

$(\mathrm{Eff}R)_{slag}$ needed for best agreement with measurements at $B_{max} = 2$ T are much lower than those at 4 T. This trend is again caused by cathode wall nonuniformities. At the same diagonal load resistance, the observed lengths of shorted slag groups on the cathode wall are substantially longer at 2 T than at 4 T. Petty has hypothesized that the resegmentation phenomena of cathode wall slag layer are caused by concentrated local Joule heating.[8] The Joule heating arises either from the constrictions of Faraday currents near the downstream edge of shorted electrode groups or from the axial current within the slag layer. The current concentrations cause local removal or thinning of the slag and create "open" gaps capable of sustaining the Hall voltage. At the reduced magnetic field strength, much longer slag resegmentation pitches are required before the current constrictions can build up enough strength to create the "open" gaps.

A typical streamwise variation of the static pressure at $B_{max} = 2$ T is shown in Fig. 12 to illustrate the normal shock model in the analysis. Best agreement with pressure measurements occurred when the shock recovery in the analysis is assumed to be ~95% of the normal shock recovery.

The effective slag layer resistance under actual power generating conditions is strongly influenced by the cathode wall nonuniformities. Consider Fig. 13 where the values of $(\mathrm{Eff}R)_{slag}$ used in the analysis, which gave best agreement with measurements, are plotted vs some parameter that characterizes the observed extent of cathode nonuniformity. The number of high-voltage cathode gaps, which collectively sustain 85% of the total Hall voltage, was chosen in Fig. 13 as a measure of nonuniformity effects. The results for different combinations of generator operating parameters (i.e., N/O, R_{link}, B_{max}, and I_{LD}) are shown in this figure. A strong correlation exists between the value of $(\mathrm{Eff}R)_{slag}$ and the number of working gaps on the cathode wall. The fact that the values of $(\mathrm{Eff}R)_{slag}$ do not lie on a single curve implies that the various generator operating parameters can influence $(\mathrm{Eff}R)_{slag}$ through other mechanisms in addition to cathode nonuniformity effects. For example, comparing cases with a comparable amount of cathode nonuniformity (along any imaginary vertical line in Fig. 13), the effective slag layer resistance decreases with decreasing values of R_{LK} and B.

A first attempt has been made to curve-fit the results of $(\mathrm{Eff}R)_{slag}$ into expressions that will be useful for diagonal generator performance predictions. In Fig. 14, the results obtained from the present data analysis of Reference Channel No. 3 diagonal generator tests are compared to the following expression

$$(\mathrm{Eff}R)_{slag}^{-1}\frac{p}{2[D+H]} = 0.01 + 0.3\exp[-3.75V_{Hall}/L] \quad (30)$$

where L and V_{Hall} are the channel length (m) and measured Hall voltage (kV), respectively. Results of Fig. 14 suggest that, to a first-order approximation, $(\mathrm{Eff}R)_{slag}$ in the Reference Channel No. 3 generator correlates only to the Hall voltage. Additional efforts to find better expressions for $(\mathrm{Eff}R)_{slag}$ are currently in progress. Attempts will also be made to include results from Faraday generator experiments.

Table 1 Comparison of CDIF bare wall diagonal generator test data with results of analysis

	Data	Calculation
Power delivered to diagonal load (kW)	811.0	812.0
Power dissipated in link resistors (kW)	—	102.0
Hall voltage (kV)	7.1	7.1
Total channel wall heat loss (MW)	5.3	5.9
Peak averaged electrode current (A)	~13.5	12.2
Peak averaged axial field (kV/m)	~2.4	2.31
Wall temperature (K)	—	1000.0

Experimental conditions
Mass flow rate = 5.97 kg/s
N/O = 0.98
B_{max} = 2.92 T
Seed flow rate ≃ 2 wt. % K
Diagonal load current = 115 A
Linkage resistance = 4 Ω
Number of electrode overlap = 16

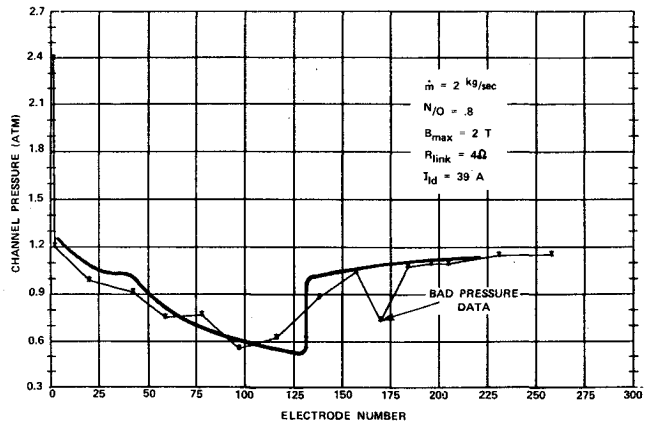

Fig. 12 Comparison of measured and calculated static pressure distributions.

Data Analysis of the CDIF Diagonal Generator Tests

The CDIF diagonal generator results obtained from the bare wall tests[3] of Oct. 14, 1982, and the slagged wall tests[4] of Dec. 16, 1983, have been compared with computer analyses. The calculational procedure was the same as that for the Reference Channel No. 3 generator data analysis.

A comparison of calculated and measured results for the bare wall test is shown in Table 1. The metal wall temperature is not known a priori in the bare wall channel calculations. Results of generator calculations for various assumed values of wall temperature were compared with measured data. The temperature of 1000 K was selected because these results agreed best with the measured power output, Hall voltage, and channel heat loss. This wall temperature is probably the surface temperature of the seed that condenses on the walls of the generator. Additional comparisons between calculated and measured results can be found in Ref. 13.

The comparisons of calculated and measured results for the slagged wall tests are shown in Fig. 15. The measurements were taken at four different operating conditions during the diagonal generator test. Between the operating conditions denoted by the ● and the ■, the combustion stoichiometry was optimized to maximize power output while the inverter was used to maintain the diagonal load voltage at 6 kV. The stoichiometry was then kept constant during the subsequent inverter sweep to lower voltages. The values of the effective slag layer resistance, as inferred from the calculation/measurement comparisons, decreased only slightly as the inverter voltage is decreased. This behavior did not agree with the Avco Reference Channel No. 3 results, where the effective slag resistance decreased more substantially as V_{Hall} was reduced.

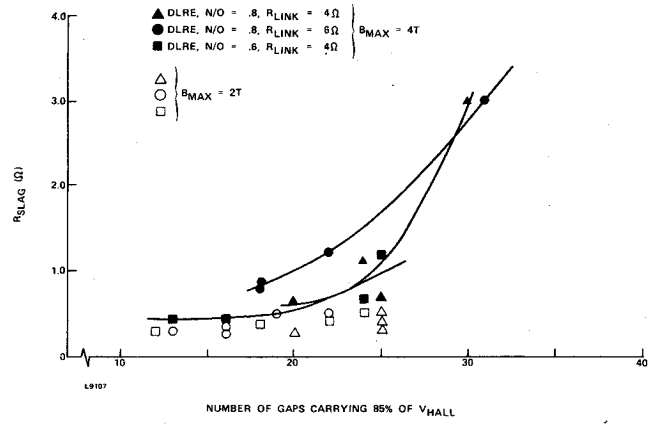

Fig. 13 Comparison of $(\mathrm{Eff}R)_{slag}$ as implied from comparative analyses with the observed number of working gaps on the cathode wall.

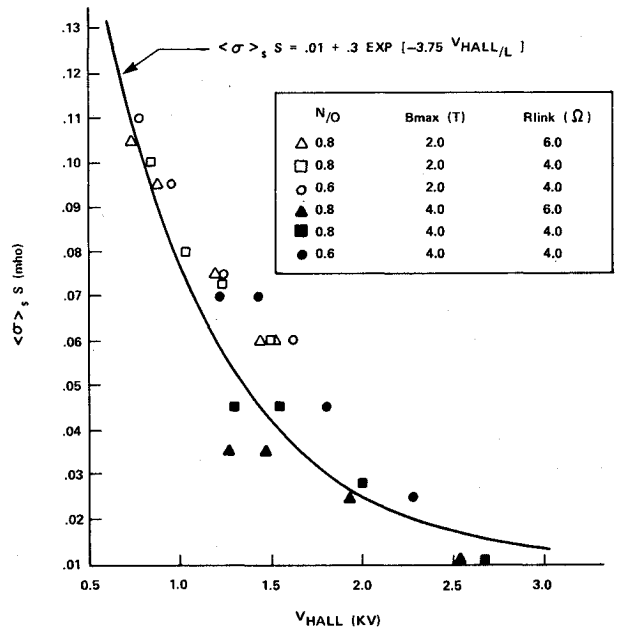

Fig. 14 Variation of $S\langle\sigma\rangle_s$ with V_{Hall} for the Ref. Channel No. 3 diagonal generator tests.

The differences in the variations of $(\mathrm{Eff}R)_{slag}$ for the two sets of diagonal generator tests might be due to dissimilarities in ash injection rates, test procedures, or test durations.

The simulated ash carry over rates of the two tests were not identical. The CDIF tests simulated 10% ash carry over while the Avco tests were in the range of 5–10%. The ash carry over rate can be very influential on the amount of cathode slag layer resegmentation.[8,14] Higher carry over rates will reduce the amount of nonuniformities. Identical ash properties cannot be assured even though both tests used Rosebud coal ash. Large variations in properties are not uncommon in natural coal slags.

The loading regimes of the two diagonal tests were different. The Reference Channel No. 3 experiments were for loading conditions on the open circuit side of the maximum power condition (Figs. 5, 6, 10, and 11); CDIF results of Fig. 15 were toward the opposite end of the load line. Since the degree of cathode wall nonuniformities are dependent on the current and voltage levels within the generator, it is quite

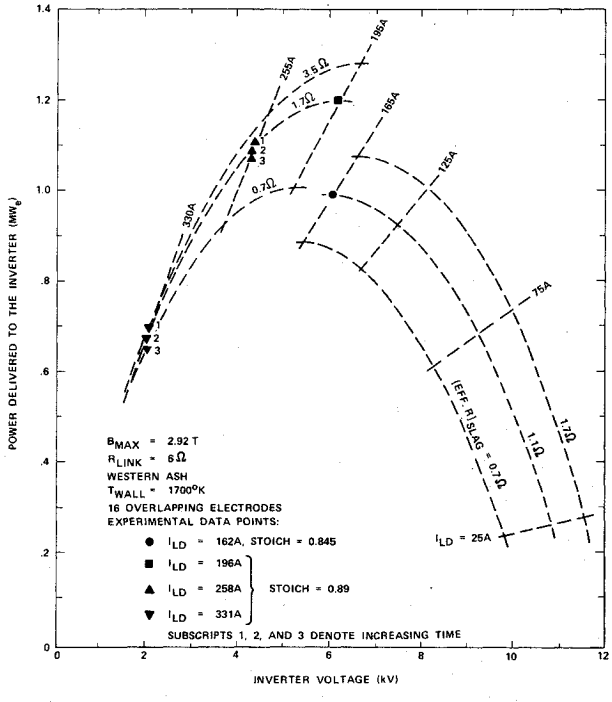

Fig. 15 CDIF 1A1-diagonal mode, December 16, 1983 experimental runs.

possible that the variation of effective slag layer resistance will not hold to the same degree on different ends of the operating load line.

The CDIF data showed that the generator did not operate sufficiently long to reach steady state at the low diagonal voltage conditions (V_{Hall} ~2 and 4 kV). The measured MHD power output continuously decreased during the run at each of these operating conditions. The temporal variations in the power output and Hall voltage are shown in Fig. 15 and are denoted by subscripts 1-3. This trend indicates that the cathode wall nonuniformities and/or other slag/wall leakage effects were probably still developing. Lower values of effective slag layer resistance might have resulted had the generator run for longer times at these two operating conditions.

Summary

The data from diagonally connected, two-terminal generator experiments in the Avco Mk VI facility and at the CDIF have been compared with analyses. From these comparisons, the effective slag layer resistance can be inferred as a function of the various generator operating parameters. The cathode slag polarization was found to be the most important effect on the effective axial slag impedance of the generator.

Slag layer leakage and cathode wall nonuniformity can affect the performance of the Reference Channel No. 3 diagonal generator by as much as 20-25%, depending on the operating conditions. These slag effects are expected to have much smaller influences on powerplant size generators.[8]

The effective slag layer resistances for the CDIF diagonal generator tests were higher than those in the Reference Channel No. 3 channel tests. This discrepancy might have arisen from differences in the ash flow rates, test procedures, and test durations.

Acknowledgment

This work was supported by the U.S. Department of Energy under Contract DE-AC22-84PC70507.

References

[1]McClaine, A. W. et al., "Performance Characteristics of a Subsonic MHD Generator Loaded in the Diagonal Mode," *21st Symposium on Engineering Aspects of MHD,* Argonne, IL, June 1983.

[2]Avco Everett Research Laboratory, Inc., Quarterly Progress Report, "MHD Generator Component Development," Contract DE-AC22-80ET15614, Aug. 1983.

[3]Farrar, L. C., "Test Report: Inverter Testing, July 7, 1982 to October 15, 1982," Mountain States Energy, Butte, MT, 2DOE-MHD-D97, June 1983.

[4]Rogers, B. B., "Diagonal Mode Channel Characterization Test Report," Mountain States Energy, Butte, MT, 2DOE-MHD-D105, Sept. 1984.

[5]Petty, S. W. et al., "Electrode Phenomena in Slagging MHD Channels," *16th Symposium on Engineering Aspects of MHD,* Pittsburgh, PA, May 1977.

[6]Demirjian, A. M. et al., "Electrode Development for Coal Fired MHD Generators," *17th Symposium on Engineering Aspects of MHD,* Stanford, CA, March 1978.

[7]Koester, J. K. and Nelson, R. M., "Electrical Behavior of Slag Coatings in Coal-Fired MHD Generators," *16th Symposium on Engineering Aspects of MHD,* Pittsburgh, PA, May 1977.

[8]Petty, S. W., "Effects of Cathode Slag Polarization on MHD Generator Performance," *21st Symposium on Engineering Aspects of MHD,* Argonne, IL, June 1983.

[9]Pian, C. C. P., Sadovnik, I., and McClaine, A. W., "Analytical Investigations of the Effects of Cathode Nonuniformities on MHD Generator Characteristics," *8th International Conference on MHD Electrical Power Generation,* Moscow, Sept. 1983.

[10]Sadovnik, I. and Pian, C. C. P., "Cathode Wall Nonuniformities in MHD Generators—Modeling and Comparison with Experiments," *23rd Symposium on Engineering Aspects of MHD,* Somerset, PA, June 1985.

[11]Gertz, J. et al., "Modeling of MHD Channel Boundary Layers Using an Integral Approach," *18th Symposium on Engineering Aspect of MHD,* Butte, MT, June 1979.

[12]Pian, C. C. P. and McClaine, A. W., "Techniques for the Solution of MHD Generator Flows," *Computers and Fluids,* Vol. 12, No. 4, April 1984.

[13]Pian, C. C. P., "Data Analysis of Diagonally-Connected Magnetohydrodynamic Power Generator Experiments," AIAA Paper 86-0129, *AIAA 24th Aerospace Sciences Meeting,* Reno, NV, Jan. 1986.

[14]Kusaka, Y. et al., "Experiments of ETL Mark VII MHD Facility," *22nd Symposium on Engineering Aspects of MHD,* Mississippi State University, Starkville, MS, June 1984.